Non-destructive, Contactless and Real-Time Capable Determination of the α′-Martensite Content in Modified Subsurfaces of AISI 304

Lara Vivian Fricke[1] · Susanne Elisabeth Thürer[1] · Moritz Jahns[2] · Bernd Breidenstein[3] · Hans Jürgen Maier[1] · Sebastian Barton[1]

Abstract

Cryogenic turning can be used to produce deformation-induced martensite in metastable austenitic steels. Martensite exhibits a higher hardness than austenite and increases the wear resistance of the workpiece. In order to reliably induce a desired martensite content in the subsurface zone during the turning process, a non-destructive, contactless and real-time testing method is necessary. Eddy current testing is an electromagnetic method that is non-destructive, non-contact and real-time capable. Furthermore, eddy current testing has been integrated into production processes many times. Eddy current testing can be used to detect the transformation of paramagnetic austenite to ferromagnetic α′-martensite based on the change in magnetic and electrical properties. Thus, the newly formed subsurface can be characterized and the manufacturing process can be monitored. The objective of this study was to understand the correlation of eddy current testing signals with newly formed α′-martensite in the subsurface of AISI 304 and to quantify the amount formed. The measurements were performed within a machining center. Several methods for reference measurement of martensite content are known in the literature. However, depending on the method used, large discrepancies may occur between the determined contents. Therefore, different analytical methods were used for reference measurements to determine the total martensite content in the subsurface. Metallographic sections, magnetic etching, Mössbauer spectroscopy, and X-ray diffraction with two different analytical methods were employed. Based on the correlation between the eddy current testing signals and the α′-martensite content in the subsurface, process control of the manufacturing process can be achieved in the future.

1 Introduction

A hardened subsurface increases the wear resistance of the surface [1]. However, due to the low carbon content and the amount of other alloying elements, stable austenitic stainless steels cannot be hardened by rapid cooling in a heat treatment process. Therefore, it would be of great benefit if a hardened subsurface zone could be produced by a machining process.

Cryogenic turning has been researched as a manufacturing process for over 10 years to develop an alternative manufacturing route for hardened metastable austenitic steels [1–8]. Metastable austenitic steels can be hardened by cryogenic machining by taking advantage of the deformation-induced martensite transformation in the subsurface zone. In addition, the surface hardness is increased by strain hardening mechanisms, resulting in increased wear and fatigue resistance [3, 4].

In order to control the evolution of the microstructure, it is important that the microstructure of the subsurface can be characterized during the process. To be able to control the cutting process, a non-destructive testing method would be most useful. Often a Feritscope is used in order to determine the content of a ferromagnetic phase [9–11]. Talonen et al. found that using a factor of 1.7 it is possible to convert the determined ferromagnetic content into the martensite content

✉ Lara Vivian Fricke
  fricke@iw.uni-hannover.de

[1] Institut für Werkstoffkunde (Materials Science), Leibniz University Hannover, 30823 Garbsen, Germany

[2] Institute of Inorganic Chemistry, Leibniz University Hannover, 30167 Hannover, Germany

[3] Institute of Production Engineering and Machine Tools, Leibniz University Hannover, 30823 Garbsen, Germany

[12]. This was determined based on experimental results and it needs adaption for different steels analyzed since their magnetic properties may vary. Additionally, this testing method is not contactless and cannot be integrated into a machine tool. Eddy current testing is an electromagnetic non-destructive testing method that which can be used contactless and in real-time. An excitation coil generates an alternating magnetic field, which induces eddy currents in an electrically conductive material. The generation and propagation of eddy currents depends on the magnetic and electrical material properties. Eddy currents generate an opposing secondary magnetic field, which is superimposed on the primary magnetic field. The resulting magnetic field induces a voltage in the measuring coil, which is measured and further evaluated. In the present study, the higher harmonic signal components were evaluated for the characterization of the magnetic material properties using a Fast Fourier Transform (FFT). This is referred to as harmonic analysis of eddy current signals. It is often used for material characterization and non-destructive determination of mechanical properties [5, 13, 14].

The particular suitability of higher harmonic analysis for the evaluation of magnetic properties is due to the different material behavior of paramagnetic and ferromagnetic phases. In the paramagnetic material state, the relative magnetic permeability μ_r exhibits a constant value, so that there is a linear relationship between the magnetic field strength and the flux density. Thus, a sinusoidal excitation current leads to an undistorted sinusoidal measured voltage. Consequently, the measurement signal demodulated by FFT exhibits only the base frequency of the excitation magnetic field, i.e. the 1st harmonic, but no higher-harmonic signal components. In the ferromagnetic state, there is a nonlinear relationship between the magnetic field strength and the magnetic flux density due to the magnetic hysteresis. This leads to a distorted measurement signal and the formation of higher harmonics of the test frequency in the measurement signal in addition to the 1st harmonic. After demodulation of the measurement signal, the base frequency and the higher harmonic signal components can be evaluated separately with respect to their amplitude and phase [5, 15, 16].

Eddy current sensors were already integrated in manufacturing processes [17, 18]. Thus, it is a promising tool to be integrated into a machine tool in order to determine the microstructure development in real-time. For such an approach, a correlation is necessary between the induced voltage and the deformation induced α'-martensite formation [10–12, 19]. Thus, reference measurements need to be conducted by ex-situ measurement methods. The determination of the martensite content is possible using X-ray diffraction (XRD), metallographic micrographs, electron backscatter diffraction and many more [2–4, 11, 19–21]. Especially, the determination of the content of a specific phase in a

subsurface is challenging, since only a small volume fraction of the sample is modified and the martensite content decreases with increasing depth. Most studies analyzing the correlation between the ferromagnetic content of a sample and electromagnetic measurement results are evaluating bulk samples, e.g. [11, 19, 21–26]. These data are not directly applicable to thin subsurface layers, and thus a comparison of different methods for the determination of the created subsurface martensite content by cryogenic external turning is presented here. The determined martensite content can then be used to create a correlation between the eddy current testing measurement signals and the subsurface microstructure to develop a non-destructive measurement system.

2 Materials and Methods

2.1 Material

The experiments were conducted using an AISI 304 metastable austenitic steel, which was solution annealed at 1050 °C for 45 min and slowly cooled in the furnace to obtain a homogeneous microstructure. The measured alloying composition was 0.028 wt% C, 0.492 wt% Si, 1.90 wt% Mn, 18.24 wt% Cr, 0.406 wt% Mo, 7.95 wt% Ni, and 0.093 wt% N and Fe balance.

2.2 Cryogenic External Turning

The cutting experiments were performed on a DMG MORI CTX 800 4A turning center. Different contents of martensite were generated by specific adaptations of the process parameters, see Table 1. The temperature of the samples was set between − 196 °C and room temperature. For the low temperature experiments, the specimens were cooled in a container filled with liquid nitrogen until the desired temperature was reached. Via a hole in the core of the specimen, the temperature was measured with a type K thermocouple directly before insertion into the lathe. No further coolant or lubricant was applied during the turning process. After machining, the temperatures within the core were about 10 °C higher than prior to machining. The cutting feed was varied between 0.2 and 1 mm, the cutting depth between 0.2 and 1.5 mm, the cutting edge between 10 and 55 μm and the cutting speed between 30 and 150 m/min. In total, 59 samples were produced, which featured different martensite subsurface contents.

2.3 Metallographic Analysis

For detailed metallographic analyis, four representative samples were chosen. They represent a wide range of the possible martensitic transformation. As described in [5, 6, 9] the

Table 1 Processing parameters

Cutting start temperature, °C	Cutting feed, mm	Cutting speed, m/min	Cutting depth, mm	Cutting edge, µm
− 196, − 150, − 100, − 70, − 40, 20	0.2, 0.6, 0.8, 1.0	30, 50, 70, 90, 110, 130, 150	0.2, 0.35, 0.5, 1.0, 1.5	10, 25, 45, 55

cutting start temperature and cutting feed show the greatest influence on the martensitic transformation by cryogenic cutting. All chosen samples for the detailed characterization were produced using a cutting edge of 10 µm, a cutting speed of 150 m/min and a cutting depth of 0.2 mm. The cutting feed for three of the chosen samples was set to 0.2 mm, and the cutting start temperature was − 196 °C, 40 °C and 20 °C. One of the chosen samples was produced using a cutting feed of 1 mm and a cutting start temperature of − 100 °C. The four samples were ground with 2500 grit SiC abrasive paper and then polished with 1 µm diamond particles. Finally, the samples were oxide polished using Eposil M-11 by QATM. After polishing of the samples, Beraha II color etchant (distilled water, hydrochloric acid, ammonium hydrogen difluoride) was applied, and images were captured with a Leica DM4000M microscope.

For scanning electron microscopy (SEM), the samples were etched after polishing using V2A stain. For SEM work, a Zeiss Supra 55VP with a beam energy of 20 kV was used.

2.4 Magnetic Etching

In addition to the Beraha II etching, magnetic etching was conducted on the four samples. With magnetic etching, ferromagnetic phases can be detected reliably [27]. Since only α'-martensite is ferromagnetic in the material analyzed, it is a suitable reference method when evaluating the different characterization techniques. Magnetic etching was done by placing a polished sample on a permanent magnet and applying a ferrofluid containing ferromagnetic particles (particle size 1 nm, type M-FER-10). The ferromagnetic particles align with the ferromagnetic parts of the samples under study, which then results in contrast in the optical images.

2.5 X-ray Diffractometry

X-ray Diffraction (XRD) was conducted with CrKα radiation (30 kV, 35 mA) on a XRD 3003 TT diffractometer system from GE Inspection Technologies. The diffraction patterns were each recorded in the range of $2\theta = 50°$ to 164.9° with a step size of 0.1° and 96 s measurement time per step. The martensite content was obtained on the one hand by a heuristic method developed by G. Faninger and U. Hartmann for all 59 samples [28]. Here the average value Q of the ratio of the intensities of martensite and austenite of different crystallographic planes was determined as:

$$Q = \frac{100\%}{\frac{J_{\alpha'}}{J_\gamma} \cdot \frac{R_\gamma}{R_{\alpha'}+1}} \tag{1}$$

J are the intensities of the measured peaks for γ-Fe (111), γ-Fe (200), γ-Fe (220), α'-Fe (110), α'-Fe (200) and α'-Fe (211). Thereby, each γ plane is set into relation with each α plane and the mean value of all data is then calculated. The R-factors were determined by Faninger and Hartmann for different steel microstructures and excitation beam sources. For AISI 304 with a lattice parameter of 3.66 Å for γ-Fe and 2.86 Å for α'-Fe, the parameters at room temperature can be obtained from Table 2a and 2b in Ref. [28].

With this approach, the martensite content was derived for each crystallographic plane ratio. Afterwards, the average over all crystallographic planes was calculated. However, by turning, a texture is created within the samples and therefore, high standard deviations were obtained for the different crystallographic planes. Additionally, it must be kept in mind that only two phases can be set into relationship. Any additional phase cannot be considered by this method. Thus, all diffractograms in the present study only give the ratio between the α'-martensite and the austenite γ content.

Additional analyses were done using the Rietveld refinement method, which is suitable for samples with overlapping reflections of various phases. Here eight samples were chosen. The cutting start temperature was varied between − 196 °C and room temperature. The cutting feed was set to 0.2 mm. Three of the samples were cut at − 100 °C using a cutting feed of 0.6 mm, 0.8 mm and 1 mm. By measuring a LaB$_6$ standard with the XRD instrument, the parameters, such as the receiving slit width, for the refinement of the steel samples were determined. For the analysis, the software Topas Version 4.2 was used, taking a texture of the different phases into account. Austenite (Fm$\bar{3}$m, $a \approx 3.618$ Å), α'-martensite (Im$\bar{3}$m, $a \approx 2.819$ Å) and an unknown phase (P63/mmc, $a \approx 2.520$ Å, $c \approx 4.120$ Å) were used to provide the initial lattice parameters for the refinement.

To obtain the desired information as a function of the distance to the surface, 10–30 µm were removed by etching before a new measurement was conducted. The results obtained were then integrated to evaluate the average volume martensite content within the subsurface.
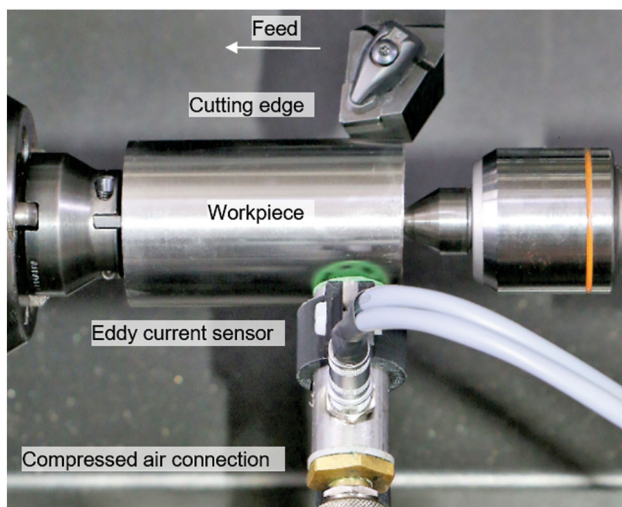
Fig. 1 Eddy current sensor integrated into the lathe

2.6 Mössbauer Spectroscopy

Mössbauer spectroscopy of ^{57}Fe was done with a ^{57}Co source embedded in an Rh matrix using backscattering geometry due to the thickness of the sample. The four samples described in Sect. 2.3 were analyzed. The measurements were done with the MIMOS II instrument manufactured at Universität Mainz equipped with four Si-Pin detectors to detect the emitted γ-photons [29–31]. The resonant 14.41 keV emission line was selected causing a penetration depth of about 500 μm. The movement of the source was adjusted to match a maximum Doppler velocity of $\pm$ 10.27 mm/s. The data were fitted using Recoil programmed at the University of Ottawa. A Lorentzian site analysis was carried out to obtain the Mössbauer parameters containing iron phases. Mössbauer parameters were then corrected to the isomer shift caused by the source matrix [32].

2.7 Eddy Current Testing

For eddy current testing a custom-built sensor was used [5]. The sensor can be cooled by compressed air to allow a high excitation current, and thus a strong primary magnetic field. All 59 samples were measured using eddy current testing. The measurements were conducted using an excitation frequency of 800 Hz and an excitation current of 2 A. Figure 1 shows the eddy current sensor inside the lathe along with workpiece and the cutting tool. Using a second revolver, the sensor was moved parallel to the cutting edge. This setup was already used in previous work for in-situ measurements [33].

3 Results and Discussion

To compare the different analyzing methods, four samples were chosen which had a wide spectrum of martensite content.

3.1 Metallographic Micrographs

In Fig. 2a and b a sample machined at a temperature of $-$100 °C with a feed of 1 mm is displayed. Figure 2a shows an SEM picture and Fig. 2b is a micrographs of the same sample etched with Beraha II. The austenite is colored blue and the martensite as well as deformation lines and twins are black. When using this etching method, martensite can hardly be distinguished from other deformation products [6].

Additionally, a yellow layer in the first micrometers of the subsurface is observed in Fig. 2b. From the SEM picture in Fig. 2a it appears that this area seems to be austenitic. Due to the machining process high working temperatures exist in the direct contact zone of the cutting tool and the workpiece. Thus, it is concluded that the martensitic transformation in the top layer is suppressed as a result of the high temperature. Mayer et al. observed the same in their study [9]. The higher the feed, the higher the temperature. Therefore, the austenitic layer direct at the surface seems to decrease with less feed and a lower cutting temperature, cf. Figure 2c and d. The first martensitic layer, which can be seen in the SEM pictures, is denser and more homogeneous when induced upon machining at a higher feed.

3.2 Magnetic Etching

Looking at Fig. 3, the denser martensitic layer for an increased feed becomes even more obvious. In Fig. 3, magnetic etched samples are displayed. The micrographs 3a and d were taken with polarized light. The ferrofluid appears brown to black depending on the amount of the deposition. For the lower cutting feed, the martensitic layer is more inhomogeneous and martensitic islands are formed. For the higher feed, the martensitic layer is contentious. For the sample machined with a lower cutting feed the martensitic transformation takes mostly place at shear bands, see Fig. 3c. It is well known that shear bands are nucleation points for the martensitic transformation [34, 35].

Due to the higher forces induced by the higher feed, the energy provided for the martensitic transformation is high enough so that a dense martensitic layer is formed. Thus, at higher cutting feeds, a more homogeneous layer can be obtained. However, with increasing feed tensile residual stresses remain in the surface [5, 9]. The high friction and hence thermal load near the surface leads to tensile stresses [9], which increase with increasing feed. Moreover, the surface is rougher [9] due to deeper feed marks. For lower feeds
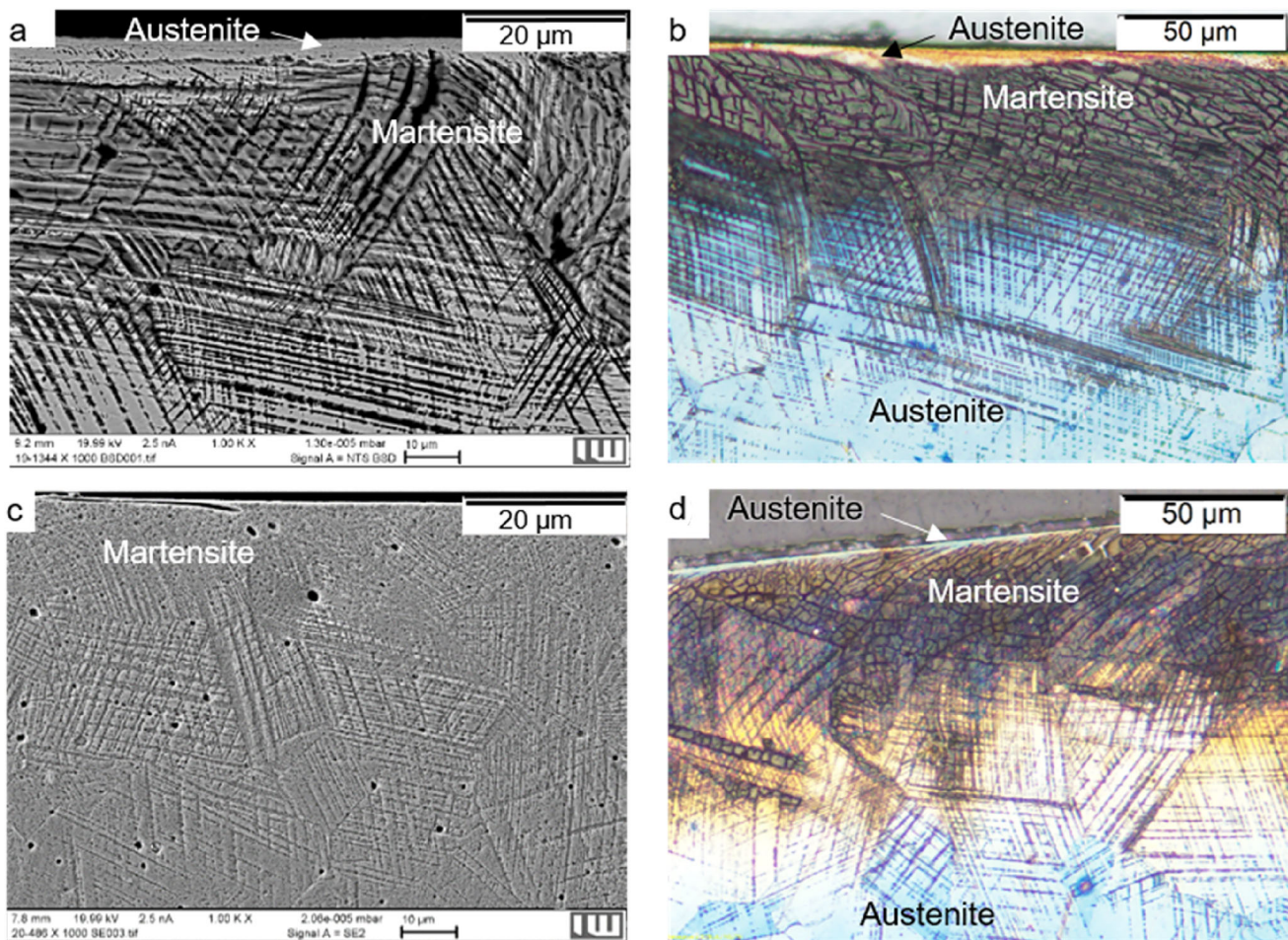
Fig. 2 **a** SEM picture and **b** Beraha II etched cross section of a sample machined at − 100 °C starting temperature and 1.0 mm feed, **c** SEM picture and **d** Beraha II etched sample machined at − 196 °C starting temperature with 0.2 mm feed

at lower temperatures the transformation takes place at energetic favorable points like shear bands. However, the energy of the cutting force is not consumed by a first, dense martensitic layer, and thus the transformation takes place up to greater depth. Further, if no cooling is applied, cf. Figure 3a, the non-transformed austenitic layer gets wider due to the higher contact temperature.

The martensite content for the etched samples was determined from the optical images using the phase analysis tool within the software Stream Enterprise. The areas marked in red in Fig. 4b and d are the martensite. Five different micrographs were analyzed for each sample. Mean values and standard deviations of the martensite contents are displayed in Table 2. Yet, the software cannot distinguish between martensite, twins and deformation lines, which all appear black when using Beraha II. Due to the fine morphology of the α'-martensite, which is very finely dispersed and formed on shear bands of the austenite phase, inaccuracies also occur when using magnetic etching [12].

3.3 X-Ray Diffraction

In Fig. 5, the α'-martensite contents determined by XRD are shown. Figure 5a shows the results obtained with the method according to [28]. As described in chapter 3.1 and 3.2, the martensite content is lower directly at the surface of the samples. Furthermore, it shows a maximum at approximately 35 μm depth. The highest transformation depths for the samples determined reached approximately 120 μm. The martensitic content displayed in Fig. 5a is again more located directly below the surface for the sample that was machined at − 100 °C using a feed of 1 mm. For the sample machined at − 196 °C with a feed of 0.2 mm more martensite was transformed at a greater depth. Still, both samples feature a similar overall martensite content. Figure 5b shows the α'-martensite content determined using the Rietveld method. The quantitative values of the overall subsurface martensite content as a function of surface distance are given in Table 2. The dotted lines show a linear connection between the measurement points used to highlight the area underneath, which

Table 2 Quantitative martensite phase fraction determined by different analyzing methods

Cutting parameters: cutting start temperature, feed	α'-Martensite content in wt%				
	Beraha II etching	Magnetic etching	XRD [28]	XRD Rietveld	Mössbauer spectroscopy
20 °C, 0.2 mm	2 ± 1	0.2 ± 0.05	0.5 ± 0.8	0.1	0
− 40 °C, 0.2 mm	3 ± 0.9	1 ± 0.4	2.6 ± 2.6	1.5	18.5
− 196 °C, 0.2 mm	12 ± 5.5	4 ± 0.9	5.9 ± 2	3.3	42.8
− 100 °C, 1 mm	12 ± 1.6	3 ± 0.7	5.4 ± 2	2.6	26.9
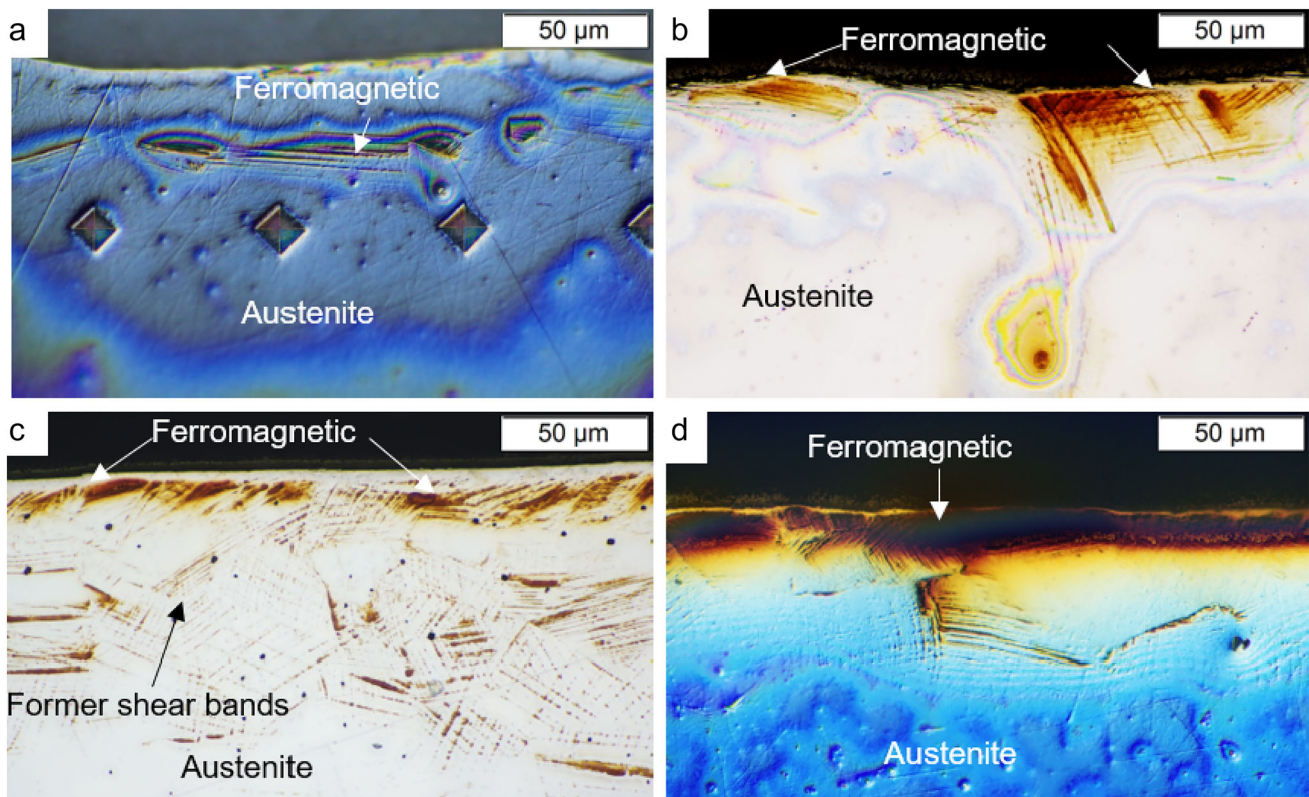
Fig. 3 Magnetic etched samples: **a** machined at 20 °C starting temperature with 0.2 mm feed, **b** machined at − 40 °C starting temperature with 0.2 mm feed, **c** machined at − 196 °C starting temperature with 0.2 mm feed and **d** machined at − 100 °C starting temperature with 1.0 mm feed

corresponds to the total α'-martensite content. It is obvious that less α'-martensite was determined in Fig. 5b when using the Rietveld method.

It should be noted that with the Rietveld method, the existence of a third phase was taken into account. It was assumed that the additional X-ray peaks belong to ε-martensite, which is likely to be formed in this steel [20, 36]. In Fig. 6 a diffractogram is shown as an example. The reflections belonging to each phase are marked. However, using the common lattice parameters in the icdd PDF-2 2016 data base, no fit was obtained. There, the lattice parameters are $a_0 = b_0 = 2.347$ Å and $c_0 = 3.797$ Å. However, Gauzzi et al. described in [37] the existence of an ε-martensite in a Fe–21%Mn–0.1%C alloy having the following parameters: $a_0 = b_0 = 2.539$ Å and c_0

= 4.095 Å. In the present study, the third phase in AISI 304 was indicated using a hexagonal phase with the parameters $a_0 = b_0 = 2.52$ Å and $c_0 = 4.12$ Å. Due to the similarity of the lattice parameters in Ref. [37] it is also assumed to be an ε-martensite. The bcc structure of the α'-martensite has the parameters $a_0 = 2.866$ Å and the fcc phase has a lattice parameter of $a_0 = 3.66$ Å, which is in the normal range for AISI 304. The grey profile at the bottom of the diffraction pattern shows the difference between the measurements (blue) and fitted data using the Rietveld method (red).

In Fig. 7, the presence of the ε- martensite as detected by XRD is shown. The phase is more present at greater depths and seams to vanish when α'-martensite is detected. This underlines the theory that the third phase is ε-martensite,
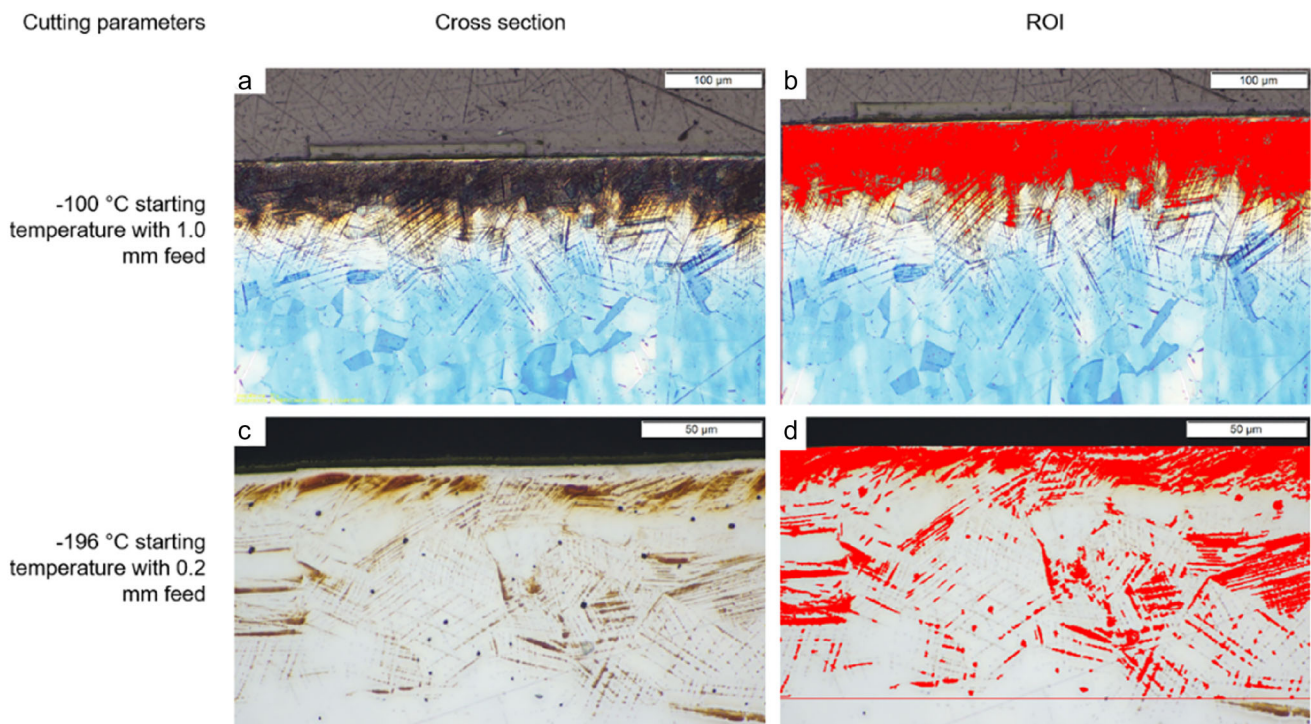
Fig. 4 Region of interest (ROI) as basis for the quantitative phase analysis (red areas are attributed to martensite): **a + b** represents the same sample, which was machined at − 100 °C starting temperature with 1.0 mm feed, the sample in **c + d** was machined at − 196 °C starting temperature with 0.2 mm feed; **a + b** Beraha II etching, **c + d** magnetic etching
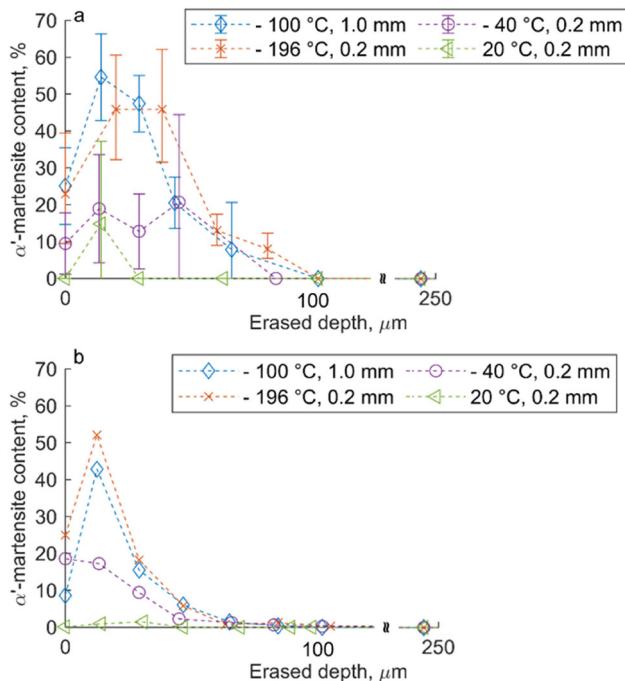
Fig. 5 α'-Martensite content as a function of distance to the surface; XRD analysis was performed according to Ref. [28] in **a** and the Rietveld method was used for **b**

since ε-martensite acts as a nucleation point for α'-martensite and then also transforms into α'-martensite [20, 35, 36]. Furthermore, Nascimento et al. found a hexagonal phase in an iron-based shape memory alloy, which has the parameters $a_0 = b_0 = 2.548(6)$ Å and $c_0 = 4.162(2)$ Å, which they labeled as ε-martensite [38]. Those parameters are also similar to the ones found in the present study.

3.4 Mössbauer Spectroscopy

In Fig. 8, Mössbauer spectra are displayed. In red the measured values are presented and in green the resulting fit is shown. Figure 8a depicts the reference measurement of an undeformed sample. For the machined samples, additional peaks appear. This is an indicator that a second α-iron phase is present [39]. The second phase in this case is α'-martensite. The greatest change in the measurement signal can be seen for the sample machined at − 196 °C, cf. Figure 8c. Hence, the largest amount of martensite was induced here.

3.5 Comparison of the Determination of the Martensite Content

The α'-martensite contents measured by each individual analyzing method are displayed in Table 2. The α'-martensite

Fig. 6 Diffraction pattern of all three phases found in AISI 304
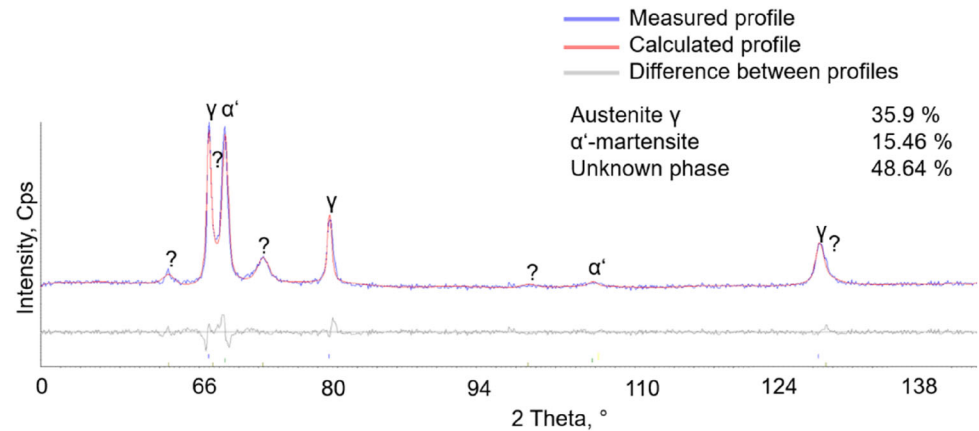
Fig. 7 α'-martensite and content of the phase assumed to be ε-martensite vs. distance to the surface depth; XRD data were evaluated using Rietveld analysis
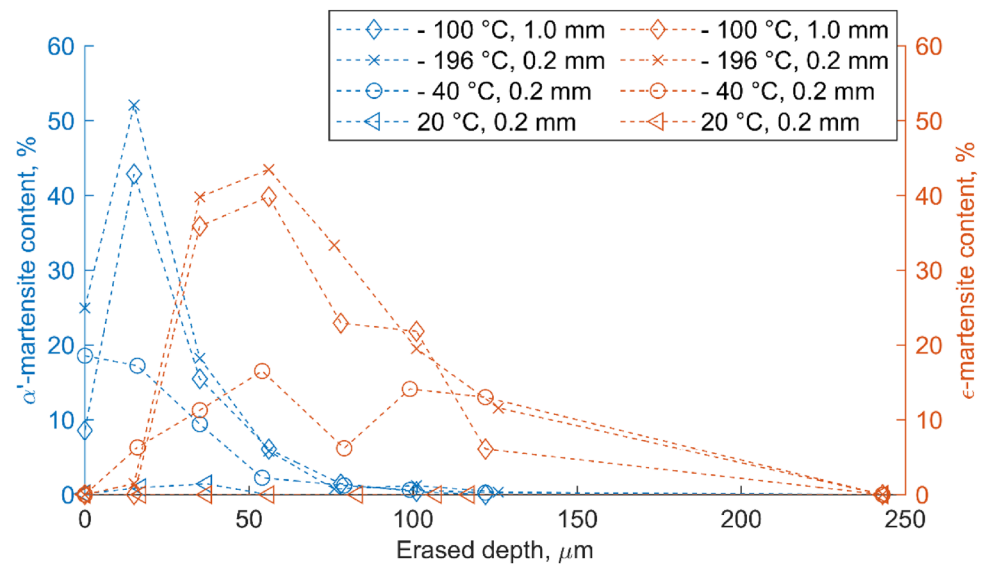
content is referred to a depth of 500 μm, because this was the measurement depth of the deepest analysis method, i.e. Mössbauer spectroscopy.

It can be seen that compared to the other reference analyzing methods, Mössbauer spectroscopy yields higher martensite contents. In the present case, Mössbauer spectroscopy overestimates the martensite content. The overestimation might be due to the small relative intensity of the doublets. This can lead to an overestimation of the measurement results.

The martensite contents determined by samples etched with Beraha II are the second largest. Again, an overestimation of the actual martensite content is likely, since not only the martensite is colored black by Beraha II. Hence, other deformation products were also counted as martensite by the software. Hausild et al. also noted that it is not possible to accurately distinguish between martensitic laths, slip lines, and deformation twins using the classical optical microscope

or a conventional SEM image. This complicates the quantification of the martensitic volume fraction by image analysis [11].

XRD results analyzed according to [28] were affected by the texture and only two phases were taken into account. The third, unknown phase, was not analyzed. Thus, an overestimation of the α'-martensite content seems to be likely as well.

The XRD results gained using the Rietveld method and the α'-martensite content by magnetic etching are similar. Magnetic etching only stains the ferromagnetic phase and with the Rietveld method it is possible to distinguish between α'-martensite and the third additional phase. Thus, the α'-martensite content determined by those two methods seems to be the most realistic ones. Talonen et al. also showed that magnetic etching is suitable for detecting α'-martensite. However, they explained that the very fine morphology of the α'-martensite phase makes quantification difficult. In addition, uneven distribution of the Ferrofluid can lead to distorted

Fig. 8 Results of the Mössbauer spectroscopy: **a** machined at −20 °C starting temperature with 0.2 mm feed, **b** machined at −40 °C starting temperature with 0.2 mm feed, **c** machined at −196 °C starting temperature with 0.2 mm feed and **d** machined at −100 °C starting temperature with 1.0 mm feed
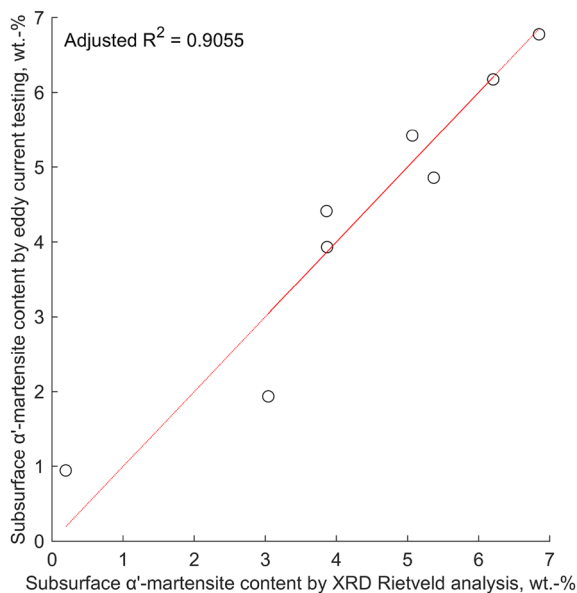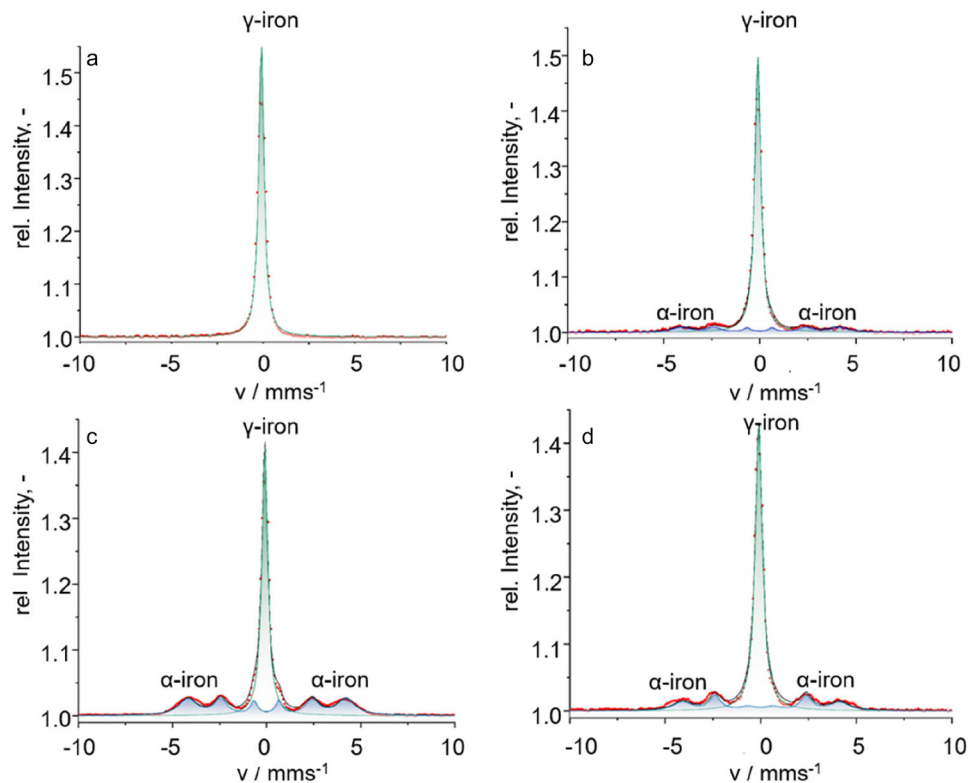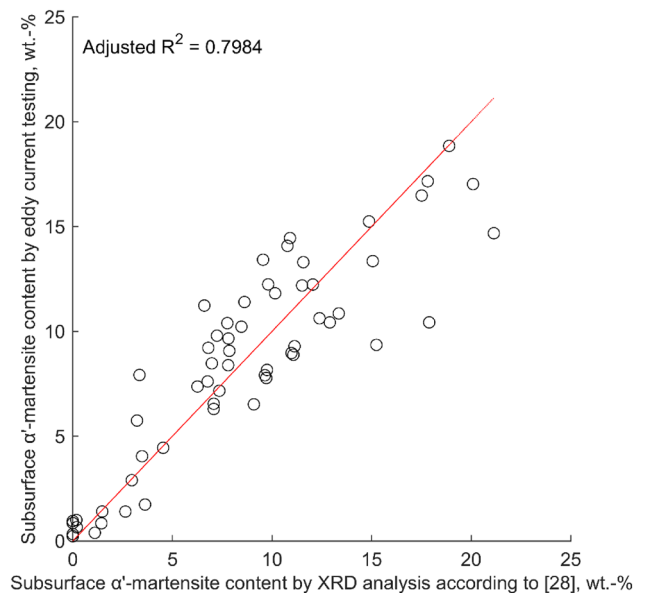

Fig. 9 Model for the determination of the α'-martensite content by eddy current testing using XRD Rietveld measurements

Fig. 10 Model for the determination of the α'-martensite content by eddy current testing based on XRD results analyzed according to [28]

images, and thus to an overestimation of the α'-martensite content [12].

3.6 Eddy Current Testing

In order to be able to develop an inline process control, it is necessary to be able to predict the martensite subsurface content by eddy current testing. Hence, a correlation between the measurement results and eddy current testing signals was created based on the experimental results. Various samples were probed after machining into the machine tool and the sensor was moved over the samples, as it would be in the
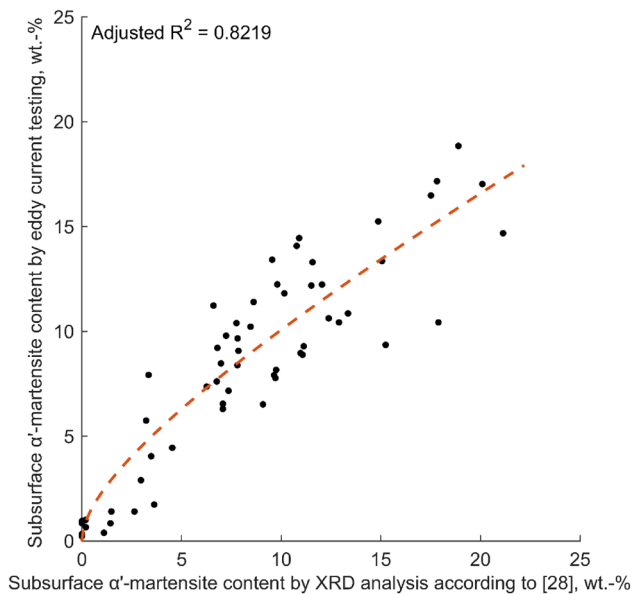
Fig. 11 Combined root and linear function for the correlation of the α′-martensite content as determined by eddy current testing

cutting process. Different models were analyzed and are compared in the following. The martensite content of the samples tested was determined by XRD using both methods previously described. Since the Mössbauer spectroscopy seems to overestimate the α'-martensite content compared to the other analyzing methods presented here, it was not considered further and the subsurface thickness to which the measurements were related was set to 243 μm. This was the greatest depth where a martensitic transformation was determined by XRD. Due to the existence of a third phase, the results of the analyzing method described by Ref. [28] appear less reliable.

In total, eight subsurface α′-martensite contents of different samples produced by cryogenic machining were determined by Rietveld analysis in this study. For the reference measurements only the α′-martensite content is important here, because ε-martensite is paramagnetic and has negligible influence on the eddy current testing used. In order to create the correlation of the eddy current testing and the martensite subsurface content, the amplitudes of the 1st (A_1) and 3rd (A_3) harmonics were used. It is important to take both amplitudes into account, since the microstructure and the total α′-martensite content have an influence on the eddy current measurement results [40]. Ahmadzade et al. also found a high correlation of the coefficients real part, imaginary part, relative modulus and relative phase angle for the 3rd harmonic and the martensite fraction [19]. The best correlation was found with a linear model, which is also in accordance with simulation results presented in [40], where a linear relationship in a specific range of martensite content was found for the amplitude of the 1st and 3rd harmonic. In the present

study, the α′-martensite content in % is obtained from the harmonic analysis of the eddy current signal as:

$$\alpha'_{\text{ET}_{\text{Rietveld}}} = -13.8 + 283.5 \cdot A_1 + 3234 \cdot A_3 - 50548 \cdot A_1 \cdot A_3 \tag{2}$$

In Fig. 9 a correlation with an adjusted R^2 of 0.9055 between the subsurface α′-martensite content and the measurement results of eddy current testing is seen. This correlation shows that with eddy current testing, a sufficiently accurate determination of the subsurface α′-martensite content can be achieved.

Next the eddy current testing results were correlated with the subsurface α′-martensite content determined by the method described by [28], see Fig. 10. Here, all 59 samples were analyzed.

In this case, an adjusted R^2 of 0.7984 was obtained for:

$$\alpha'_{\text{ET}[21]} = -49.8 + 985.3 \cdot A_1 + 11504 \cdot A_3 - 233050 \cdot A_1 \cdot A_3 \tag{3}$$

Other researchers like Hotz et al. [41] used a Feritscope to determine the α'-martensite content after machining. They calibrated the electromagnetic measurements on α'-martensite contents, determined by metallographic cross sections etched with Beraha II. They found a good correlation of $R^2 = 0.8874$. The black areas were assumed to be α'-martensite. In Fig. 4a, a metallographic cross section etched with Beraha II is shown. If all the black areas created by Beraha II etching are assumed to be α'-martensite, an overestimation of the α'-martensite content follows. Talonen et al. also found that metallographic cross sections tend to overestimate the α'-martensite content although they used magnetic etching [12]. Furthermore, Talonen et al. compared different methods for the determination of the α'-martensite content in AISI 304. They found a linear relationship between Feritscope measurements and different reference measurements like XRD, Satmagan, magnetic balance or density measurements. In the present study, the same trends were seen when evaluating the martensite content based XRD data. However, unlike Talonen et al., XRD measurements for different surface distance were obtained, and thus the total subsurface α'-martensite contents were determined. Talonen et al. only used surface measurements [12] which leads to different values because the martensite content is not constant over the depth and electromagnetic measurements probe up to a greater depth than XRD. Additionally, Talonen et al. criticized the texture influence for XRD measurements, which also lead in this study to high standard deviations. However, XRD measurements evaluated by the Rietveld method are less influenced by texture compared to other XRD evaluating methods, and thus this method appears to give the most precise information about the α'-martensite content. This is

more so, if the measurements are conducted over the interesting transformation depth. Such data can then be used for the calibration of an electromagnetic measurement method.

Most of the literature use a linear relationship between the electromagnetically determined α'- martensite content and the reference measurements. A comparison of different studies was done by Talonen et al. [12]. There it is described that the approach of Hecker et al. [42] overestimates the α'-martensite content [12]. Looking at Fig. 10, the linear approach seems to underestimate the data at higher α'-martensite contents and to overestimate smaller ones. Hence, as also conducted by Hotz et al. [41], a root function and a linear function were used to fit the data. The result is presented in Fig. 11. Here, the linear function presented in Eq. 2 was used to determine the α'-martensite content in wt%, as it is done by a different calibration function in the Feritscope and then a root function was applied to correlate the martensite content determined by eddy current testing with the reference method.

A good correlation with an adjusted R^2 of 0.8219 was achieved for:

$$\alpha'_{\text{ET}} = 1.922 \cdot \sqrt{\alpha'_{\text{ET}[21]}} + 0.3995 \cdot \alpha'_{\text{ET}[21]} \tag{4}$$

All in all it can be said that eddy current testing appears to be useful tool to determine the subsurface α'- martensite content created by cryogenic turning. This can be used as a basis for an in-process control to tailor the turning parameters to achieve a given subsurface martensite content.

4 Conclusion

Different analyzing methods were compared regarding their capability to determine the martensite subsurface content of cryogenically machined workpieces made of AISI 304. Mössbauer spectroscopy and metallographic examinations with Beraha II etched samples overestimate the martensite content. Magnetic etching and XRD analysis using the Rietveld method give the most accurate and similar martensite contents. Here, the ferromagnetic α'-martensite content can be distinguished from other phases reliably.

Furthermore, the amplitudes of the 1st and the 3rd harmonic of eddy current testing can be correlated to the subsurface α'-martensite content. XRD measurements analyzed by the Rietveld method yielded a correlation coefficient of 0.9055 for the eddy current testing. Using a root function and a higher number of XRD measurement results, a correlation coefficient of 0.8219 can be achieved. Hence, it is possible to detect the newly created subsurface martensite content contactless and in real-time by eddy current testing. Thus, this non-destructive testing method can be used as a

basis of a process control to induce the desired subsurface martensite content.

Declarations

Conflict of interest The authors declare no conflict of interest.

Consent for Publication Not applicable.

Ethical Approval Not applicable.

References

1. Frölich, D., Magyar, B., Sauer, B., Mayer, P., Kirsch, B., Aurich, J.C., Skorupski, R., Smaga, M., Beck, T., Eifler, D.: Investigation of wear resistance of dry and cryogenic turned metastable austenitic steel shafts and dry turned and ground carburized steel shafts in the radial shaft seal ring system. Wear **328–329**, 123–131 (2015). https://doi.org/10.1016/j.wear.2015.02.004

2. Hotz, H., Kirsch, B.: Influence of tool properties on thermomechanical load and surface morphology when cryogenically turning metastable austenitic steel AISI 347. J. Manuf. Process **52**, 120–131 (2020). https://doi.org/10.1016/j.jmapro.2020.01.043

3. Hotz, H., Kirsch, B., Zhu, T., Smaga, M., Beck, T., Aurich, J.C.: Surface layer hardening of metastable austenitic steel—comparison of shot peening and cryogenic turning. J. Mater. Res. **9**(6), 16410–16422 (2020). https://doi.org/10.1016/j.jmrt.2020.11.109

4. Hotz, H., Smaga, M., Kirsch, B., Zhu, T., Beck, T., Aurich, J.C.: Characterization of the subsurface properties of metastable austenitic stainless steel AISI 347 manufactured in a two-step turning process. Procedia CIRP **87**, 35–40 (2020). https://doi.org/10.1016/j.procir.2020.02.012

5. Fricke, L.V., Nguyen, H.N., Breidenstein, B., Zaremba, D., Maier, H.J.: Eddy current detection of the martensitic transformation in AISI304 induced upon cryogenic cutting. J. Iron. Steel Res. Int. (2020). https://doi.org/10.1002/srin.202000299

6. Fricke, L.V., Gerstein, G., Breidenstein, B., Nguyen, H.N., Dittrich, M.-A., Maier, H.J., Zaremba, D.: Deformation-induced martensitic transformation in AISI304 by cryogenic machining. Mater. Lett. **285**, 129090 (2021). https://doi.org/10.1016/j.matlet.2020.129090

7. Mayer, P., Kirsch, B., Müller, R., Becker, S., Ev, H., Aurich, J.C.: Influence of cutting edge geometry on deformation induced hardening when cryogenic turning of metastable austenitic stainless steel AISI 347. Procedia CIRP **45**, 59–62 (2016). https://doi.org/10.1016/j.procir.2016.02.148

8. Mayer, P., Skorupski, R., Smaga, M., Eifler, D., Aurich, J.C.: Deformation induced surface hardening when turning metastable austenitic steel AISI 347 with different cryogenic cooling strategies. Procedia CIRP **14**, 101–106 (2014). https://doi.org/10.1016/j.procir.2014.03.097

9. Mayer, P., Kirsch, B., Müller, C., Hotz, H., Müller, R., Becker, S., von Harbou, E., Skorupski, R., Boemke, A., Smaga, M., Eifler, D., Beck, T., Aurich, J.C.: Deformation induced hardening when cryogenic turning. CIRP J. Manuf. Sci. Technol. **23**, 6–19 (2018). https://doi.org/10.1016/j.cirpj.2018.10.003

10. Hauser, M., Wendler, M., Ghosh Chowdhury, S., Weiß, A., Mola, J.: Quantification of deformation induced α'-martensite in Fe–19Cr–3Mn–4Ni–0.15C–0.15N austenitic steel by in situ magnetic measurements. Mater. Sci. Technol. **31**(12), 1473–1478 (2015). https://doi.org/10.1179/1743284714Y.0000000731

11. Haušild, P., Davydov, V., Drahokoupil, J., Landa, M., Pilvin, P.: Characterization of strain-induced martensitic transformation in a metastable austenitic stainless steel. Mater. Des. **31**(4), 1821–1827 (2010). https://doi.org/10.1016/j.matdes.2009.11.008

12. Talonen, J., Aspegren, P., Hänninen, H.: Comparison of different methods for measuring strain induced α-martensite content in austenitic steels. Mater. Sci. Technol. **20**(12), 1506–1512 (2004). https://doi.org/10.1179/026708304X4367

13. Bruchwald, O., Frackowiak, W., Reimche, W., Maier, H.: Sensor-controlled bainitic transformation and microstructure formation of forgings during the cooling process. Mat.-wiss. u Werkstofftech. **47**, 780–788 (2016). https://doi.org/10.1002/mawe.201600612

14. Fricke, L.V., Skalecki, M.G., Barton, S., Klümper-Westkamp, H., Zoch, H.-W., Zaremba, D.: In-situ characterization by eddy current testing of graded microstructural evolution in the core and peripheral zone during material conversion during case hardening. HTM J. Heat Treat. Mater. **74**(6), 345–356 (2019). https://doi.org/10.3139/105.110395

15. Bruchwald, O., Frackowiak, W., Reimche, W., Maier, H.: Nondestructive in situ monitoring of the microstructural development in high performance steel components during heat treatment. La Metallurgia Italiana **11**(12), 29–37 (2015)

16. Mercier, D., Lesage, J., Decoopman, X., Chicot, D.: Eddy currents and hardness testing for evaluation of steel decarburizing. NDT & E Int. **39**, 652–660 (2006). https://doi.org/10.1016/j.ndteint.2006.04.005

17. Wolter, B., Gabi, Y., Conrad, C.: Nondestructive testing with 3MA—an overview of principles and applications. Appl. Sci. **9**, 1068 (2019). https://doi.org/10.3390/app9061068

18. Yang, H., van den Berg, F., Luinenburg, A., Bos, C., Kuiper, G., Mosk, J., Hunt, P., Dolby, M., Flicos, M., Peyton, A.J., Davis, C.L.: In-line quantitative measurement of transformed phase fraction by EM sensors during controlled cooling on the run-out table of a hot strip mill. In: 19th world conference on non-destructive testing (WCNDT 2016) in Munich, Germany, pp. 1–8. (2016)

19. Ahmadzade, E., Kahrobaee, S., Kashefi, M., Ahadi Akhlaghi, I., Mazinani, M.: Quantitative evaluation of deformation induced martensite in austenitic stainless steel using magnetic NDE techniques. J. Nondestr. Eval. **39**, 28 (2020). https://doi.org/10.1007/s10921-020-00671-8

20. Weiß, A., Gutte, H., Mola, J.: Contributions of ε and α′ TRIP effects to the strength and ductility of AISI 304 (X5CrNi18-10) austenitic stainless steel. Metall. Mater. Trans. A **47A**, 112–122 (2015). https://doi.org/10.1007/s11661-014-2726-y

21. Celada-Casero, C., Kooiker, H., Groen, M., Post, J., San-Martin, D.: In-situ investigation of strain-induced martensitic transformation kinetics in an austenitic stainless steel by inductive measurements. Metals **7**, 271 (2017)

22. Khan, S., Ali, F., Khan, A., Iqbal, M.: Eddy current detection of changes in stainless steel after cold reduction. Comput. Mater. Sci **43**, 623–628 (2008). https://doi.org/10.1016/j.commatsci.2008.01.034

23. Beese, A.M., Mohr, D.: Identification of the direction-dependency of the martensitic transformation in stainless steel using in situ magnetic permeability measurements. Exp. Mech. **51**, 667–676 (2011). https://doi.org/10.1007/s11340-010-9374-y

24. Cao, B., Iwamoto, T.: An experimental study on strain rate sensitivity of strain-induced martensitic transformation in SUS304 by real-time measurement of relative magnetic permeability. J. Iron. Steel Res. Int. **87**, 1700022 (2017). https://doi.org/10.1002/srin.201700022

25. Oršulová, T., Palček, P., Kudelcik, J.: Effect of plastic deformation on the magnetic properties of selected austenitic stainless steels. Prod. Eng. Arch. **14**, 15–18 (2017)

26. Oršulová, T., Palček, P., Roszak, M., Uhríčik, M., Smetana, M., Kúdelčík, J.: Change of magnetic properties in austenitic stainless steels due to plastic deformation. Procedia Struct. Integr. **13**, 1689–1694 (2018). https://doi.org/10.1016/j.prostr.2018.12.352

27. Gray, R.J.: Magnetic etching. In: Vander Voort, G.F. (ed.) Applied metallography, pp. 53–61. Springer, Boston (1986)

28. Faninger, G., Hartmann, U.: Physikalische Grundlagen der quantitativen röntgenographischen Phasenanalyse (RPA). Härterei-Technische Mitteilung **27**, 233–244 (1972)

29. Klingelhöfer, G., Morris, R.V., Bernhardt, B., Rodionov, D., de Souza, P.A., Jr., Squyres, S.W., Foh, J., Kankeleit, E., Bonnes, U., Gellert, R., Schröder, C., Linkin, S., Evlanov, E., Zubkov, B., Prilutski, O.: Athena MIMOS II Mössbauer spectrometer investigation. J. Geophys. Res. (2003). https://doi.org/10.1029/2003JE002138

30. Fleischer, I., Klingelhöfer, G., Morris, R.V., Schröder, C., Rodionov, D., de Souza, P.A.: In-situ Mössbauer spectroscopy with MIMOS II. In: Yoshida, Y. (ed.) ICAME 2011, pp. 533–541. Springer, Dordrecht (2013)

31. Klingelhöfer, G., Morris, R.V., de Souza, P.A., Bernhardt, B.: The miniaturized mössbauer spectrometer mimos ii of the athena payload for the 2003 mer missions. In: Sixth Int. Conf. Mars 2003, pp. 3–5. (2003)

32. Gütlich, P., Link, R., Trautwein, A.: Mößbauer spectroscopy and transition metal chemistry Mössbauer spectroscopy and transition metal chemistry: fundamentals and applications. Springer, Berlin (2011)

33. Denkena, B., Breidenstein, B., Dittrich, M.-A., Wichmann, M., Nguyen, H.N., Fricke, L.V., Zaremba, D., Barton, S.: Setting of deformation-induced martensite content in cryogenic external longitudinal turning. Procedia CIRP **108**, 170–175 (2022). https://doi.org/10.1016/j.procir.2022.03.030

34. Olson, G., Cohen, M.: Kinetics of strain-induced martensitic nucleation. Metall. Trans. A **6**, 791–795 (1975). https://doi.org/10.1007/BF02672301

35. Olson, G.B., Cohen, M.: A mechanism for the strain-induced nucleation of martensitic transformations. J. Less Common Met. **28**(1), 107–118 (1972). https://doi.org/10.1016/0022-5088(72)90173-7

36. Schumann, H.: Verformungsinduzierte Martensitbildung in metastabilen austenitischen Stählen. Krist. Techn. **10**(4), 401–411 (1975). https://doi.org/10.1002/crat.19750100409

37. Gauzzi, F., Montanari, R.: Martensite Reversion in an Fe-21%Mn-0.1%C alloy. Mater. Sci. Eng. A **57**(273–275), 524–527 (1999)

38. Nascimento Borges, F.C., Mei, P., Cardoso, L., Otubo, J.: Grain size effect on the structural parameters of the stress induced epsilon(hcp)—martensite in iron-based shape memory alloy. Mater. Re.s-Ibero-Am. J. Mater. **11**(1), 63–67 (2008). https://doi.org/10.1590/S1516-14392008000100012

39. Waanders, F., Vorster, S., Engelbrecht, A.: Mossbauer and SEM characterisation of the scale on type 304 stainless steel. Scr. Mater. **42**, 997–1000 (2000). https://doi.org/10.1016/S1359-6462(00)00322-5

40. Fricke, L.V., Nguyen, H.N., Appel, J., Breidenstein, B., Maier, H.J., Zaremba, D., Barton, S.: Characterization of deformation-induced martensite by cryogenic turning using eddy current testing. Procedia CIRP **108**, 49–54 (2022). https://doi.org/10.1016/j.procir.2022.03.014

41. Hotz, H., Kirsch, B., Aurich, J.C.: Impact of the thermomechanical load on subsurface phase transformations during cryogenic turning of metastable austenitic steels. J. Intell. Manuf. **32**(3), 877–894 (2021). https://doi.org/10.1007/s10845-020-01626-6

42. Hecker, S.S., Stout, M.G., Staudhammer, K.P., Smith, J.L.: Effects of strain state and strain rate on deformation-induced transformation in 304 stainless steel: part I. Magnetic measurements and mechanical behavior. Metall. Trans. A **13**(4), 619–626 (1982). https://doi.org/10.1007/BF02644427